Discrete Ginzburg-Landau Solitons

N.K. Efremidis and D.N. Christodoulides

Summary. In this chapter, we present a review of recent results concerning dissipative lattices of Ginzburg-Landau type. Firstly, we study effects such as complex discrete diffraction, as well as Bloch oscillations, arising from the linear properties of such systems. Subsequently, using a generic cubic-quintic nonlinearity, we identify self-localized dissipative discrete soliton solutions, and study their characteristics.

1 Introduction

The complex Ginzburg-Landau (GL) equation is known to play a ubiquitous role in science. This equation is encountered in several diverse branches of physics, for example in superconductivity and superfluidity, non-equilibrium fluid dynamics and chemical systems, nonlinear optics and Bose-Einstein condensates [1, 2, 3, 4, 5, 6]. In general, the very nature of the GL system is such that it can provide rich behavior, ranging from chaos and pattern formation to self-localized solutions or solitons. In the latter regime, GL dissipative solitons (or auto-solitons) are possible as a result of the interplay between linear/nonlinear gain, nonlinearity and complex dispersion [7, 8, 9, 10]. Over the years, the soliton solutions of the Ginzburg-Landau equation and their underlying dynamics have been the subject of intense investigation. Such pulse-like soliton states were first identified within the context of the cubic GL model [7, 8], and subsequently in the generalized quintic regime [4, 9, 10], and, typically, they represent chirped coherent structures (or one-dimensional defects) that are obtained through heteroclinic trajectories in the phase space of the stationary GL equation. Several types of solitary wave solutions of the continuous GL equation have been identified over the last few years. These include flat-top solutions in one and two dimensions [11, 12], erupting (exploding) and creeping solitons [13, 12] and spiraling solitons carrying topological charge [14, 15].

Quite recently, the behavior of nonlinear discrete optical systems has received considerable attention [16, 17]. Because of discreteness, the properties of this class of systems are artificially altered, and, as a result, their nonlinear behavior is known to exhibit features that are otherwise impossible in the bulk/continuous regime. In optics [16], nonlinear arrays of nearest-neighbor-coupled waveguides have provided a fertile ground where such discrete

N.K. Efremidis and D.N. Christodoulides: *Dissipative Solitons*,
Lect. Notes Phys. **661**, 309–325 (2004)
www.springerlink.com

nonlinear interactions of the discrete nonlinear Schrödinger-type can be experimentally observed and investigated [18]. In the presence of loss or gain, these lattices become dissipative, and can be described by discrete Ginzburg-Landau (DGL) type models. Such DGL lattices are quite often used to describe a number of physical systems, such as Taylor and frustrated vortices in hydrodynamics [19] and laser arrays and semiconductor optical amplifiers in optics [20, 21]. In these latter studies, the DGL model has been predominantly used in connection with spatio-temporal chaos, instabilities and turbulence [22]. However, discrete soliton (DS) solutions of the DGL model have not been identified until very recently [23]. In addition, discrete solitons have been identified in dissipative lattices of Ablowitz-Ladik type [24], as well as in optical cavities [25].

In this chapter, we present a review concerning the linear and nonlinear properties of Ginzburg-Landau discrete chains [23, 26]. More specifically, we first analyze the complex dispersion properties within a Brillouin zone. As a result of discreteness, the dispersion/diffraction behavior of a GL lattice differs substantially from that encountered in conservative arrays [16]. In addition, we study the effect of a linear refractive index modulation in a low-power system of active waveguides (such as laser arrays or semiconductor optical amplifier lattices), and study Bloch oscillations of complex type. In optics, Bloch oscillations have been predicted [27] and experimentally demonstrated in waveguide arrays [28, 29]. One would naturally expect that the presence of gain and loss would prevent the existence of periodic Bloch oscillations. However, as it is shown, Bloch oscillations are still possible, even though gain and loss mechanisms allow energy exchange in this system [26], and in spite of the fact that, in general, the total power will increase or decrease exponentially. For a specific choice of the parameters, the total gain compensates for the loss, and this results, on average, in a constant power envelope. This is in contrast to regular lattices with zero refractive index modulation, where either the in-phase or the π-out-of-phase evanescently-coupled modes (corresponding to the base and the edge of the first Brillouin zone) are preferentially amplified. In the nonlinear regime, we study the properties of discrete soliton solutions [23]. In general, two new types of DGL solitons can exist under the same conditions. These solutions are located either at the base or at the edge of the Brillouin zone, and they bifurcate at different values of the linear gain. Due to discreteness, the system exhibits novel features that have no counterparts whatsoever in either the continuous GL limit or in other conservative discrete models [16, 18] [as in discrete nonlinear Schrödinger (DNLS) chains]. These include, for example, on-site and intra-site bright DGL solitons that can both be stable, as well as new bifurcation types that cannot be identified in the continuous case. Approximate discrete solitons solutions, which are in excellent agreement with the numerically-found ones, are also obtained. These solutions are valid when

the discrete solitons are quite broad (occupying many lattice sites), or narrow, i.e., when most of the power is essentially located in a few lattice sites.

2 Formulation

In general, the cubic-quintic DGL equation is given by

$$\mathrm{i}\dot{u}_n - \mathrm{i}\epsilon u_n + \alpha(u_{n+1} + u_{n-1}) + p|u_n|^2 u_n + q|u_n|^4 u_n = 0 \,, \tag{1}$$

where $p = p_r + \mathrm{i}p_i$, $q = q_r + \mathrm{i}q_i$, $\alpha = \alpha_r + \mathrm{i}\alpha_i$, ϵ is a real parameter and $\dot{u}_n$ is the partial derivative of u_n with respect to space or time (depending on the specific problem). Here, without loss of generality, we will assume that $\dot{u}_n = \mathrm{d}u_n/\mathrm{d}z$. Physically, the discretization in (1) occurs by applying the tight-binding approximation (or coupled mode theory) [21, 30]. The original continuous system, which is periodic in space, is expanded into local modes whose amplitudes are described by the corresponding discrete model. In (1), α_r accounts for the energy tunneling between adjacent elements of the lattice, while its imaginary part stands for gain/loss due to coupling. The real parts of p and q represent the strengths of the cubic and quintic nonlinearities of the system, while ϵ, p_i, q_i are the linear and nonlinear gain/loss coefficients.

Within the context of nonlinear optics, the DGL equation can arise in the description of semiconductor laser arrays [21] and in semiconductor optical amplifiers [31] (due to applying a refractive index modulation along the crystal), where the quintic term can account for the gain/nonlinearity saturation of the lasing medium. The DGL equation can also describe the dynamics of an open Bose-Einstein condensate. In this case, the lattice potential is created by the interference of two optical standing waves [32] and, in this situation, solitons of the discrete nonlinear Schrödinger type are known to exist [33]. The dissipation of the Bose-Einstein condensate naturally occurs in an open condensate, while gain can result from the interaction between the condensed and the uncondensed atoms [34, 35]. Note that, in all of these cases, it is common practice to write the original saturable nonlinearity of the system in terms of a cubic-quintic expansion, and this, in turn, conveys the fundamental properties of the original model [21, 35].

3 Linear Properties

3.1 Discrete Diffraction

We begin our analysis by considering the linear dispersion properties of the DGL equation. To do so, we write

$$u_n \propto \exp(\mathrm{i}kz - \mathrm{i}\theta n) \,,$$

where $k = k_r + \mathrm{i}k_i$ is the complex propagation wave-number and θ is the wave momentum inside the lattice. The real and imaginary parts of (1) are then found to satisfy

$$k_r = 2\alpha_r \cos\theta \,, \tag{2}$$

$$k_i = -\epsilon + 2\alpha_i \cos\theta \,. \tag{3}$$

In Fig. 1, k_r and k_i are plotted as functions of θ. Equation (2) describes the dispersive properties of the lattice within the Brillouin zone, as defined in the region $|\theta| \leq \pi$. When $|\theta| < \pi/2$ and $\alpha_r > 0$, the curvature of the dispersion relation [(2)] implies that the effective diffraction of the array is normal. On the other hand, when $\pi/2 < |\theta| < \pi$ (and $\alpha_r > 0$), the effective diffraction of the array becomes anomalous, and, of course, these regimes are reversed for $\alpha_r < 0$.

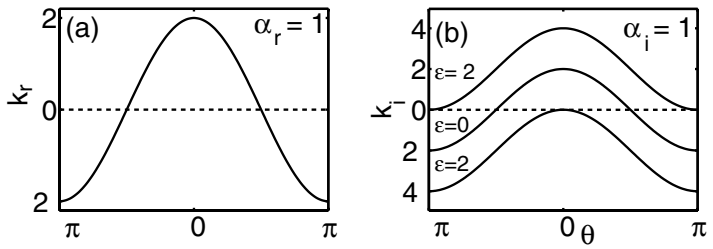

Fig. 1. (**a**) The dispersion curve for the array when $\alpha_r = 1$, and (**b**) k_i (associated with the instability growth rate) as a function of θ for $\alpha_i = 1$ and $\epsilon = -2, 0, 2$

The imaginary part of the propagation wave-number [(2)] is directly related to the growth rate of the perturbations of the "zero amplitude" solution. In particular, any perturbation frequency, θ, that satisfies the condition $k_i < 0$, will grow exponentially with a growth rate

$$g_d(\theta) = \epsilon - 2\alpha_i \cos\theta \,. \tag{4}$$

We emphasize that this growth rate is a periodic function of θ with period 2π, i.e., $g_d(\theta + 2\pi n) = g_d(\theta)$, where n is an integer. From all the possible frequencies, θ, within the Brillouin zone, only those that satisfy the inequality $\epsilon > 2\alpha_i \cos\theta$ will eventually develop instabilities. Therefore, the "zero amplitude" solution is absolutely stable for

$$\epsilon < -2|\alpha_i| \,. \tag{5}$$

On the other hand, when $\epsilon > 2|\alpha_i|$, every frequency is amplified, and the maximum growth rate (which occurs either at the base or at the edge of the Brillouin zone) is given by $\epsilon + 2|\alpha_i|$. In the regime between the two aforementioned cases, i.e., when $-2|\alpha_i| < \epsilon < 2|\alpha_i|$, only a subset of the frequencies

(i.e. those satisfying $\epsilon > 2\alpha_i \cos\theta$) will be amplified, while the rest of them will decay. Note that the instability behavior of the "zero amplitude" solution of the DGL is fundamentally different from that arising in the continuous GL limit; it is described by (Sect. 5.1)

$$g_c(\theta) = \epsilon' + \alpha_i \theta^2 \ . \tag{6}$$

Apparently, in the continuous limit, the stability properties are strongly affected by the sign of the diffusion coefficient, α_i, and, in fact, for $\alpha_i > 0$, the "zero amplitude" solution will always be unstable, regardless of the value of ϵ. Thus, in order to stabilize the background of a self-localized state, it is essential to have $\alpha_i < 0$. On the other hand, the DGL model has the interesting property that the background can be stabilized for both signs of α_i by choosing the linear gain ϵ of the system in an appropriate manner.

The linear part of (1) also supports exponentially-decaying/growing solutions of the form

$$u_n \propto \exp(\pm sn + \mathrm{i}kz) \ , \tag{7}$$

where the parameters of (7) obey

$$k = 2\alpha_r \cosh s_r \cos s_i - 2\alpha_i \sinh s_r \sin s_i \ , \tag{8}$$

$$\epsilon = 2\alpha_r \sinh s_r \sin s_i + 2\alpha_i \cosh s_r \cos s_i \ . \tag{9}$$

We would like to mention that, in the linear regime, (1) can be solved analytically. When only one lattice element is initially excited (say $n = 0$ at $z = 0$), the field profile at z is given by

$$u_n(z) = u_0 J_n(2\alpha z) \mathrm{e}^{\mathrm{i}\pi n/2} \mathrm{e}^{\epsilon z} \ , \tag{10}$$

where $J_n(x)$ (with complex argument) is a Bessel function of the first kind with integer order n. The evolution of more involved initial field patterns can be readily obtained by simple superposition from this impulse response. In Fig. 2a–d, the impulse response of the lattice at $z = 3$ is depicted for $\alpha = 1, 1+i, i, -i$, respectively. In Fig. 2c, the out-of-phase mode is preferentially amplified, while in Fig. 2d, the mode is in-phase at the output.

3.2 Bloch Oscillations

Bloch was the first to show that an electron wavefunction has the tendency to periodically revive when an external potential is applied to the periodic lattice of a solid [36]. In optics, Bloch oscillations were predicted [27] and have been experimentally demonstrated in waveguide arrays [28, 29]. Let us introduce a linear refractive index modulation in a waveguide array or an additional linear potential in a Bose-Einstein condensate. In this case, the evolution of a low power field will obey

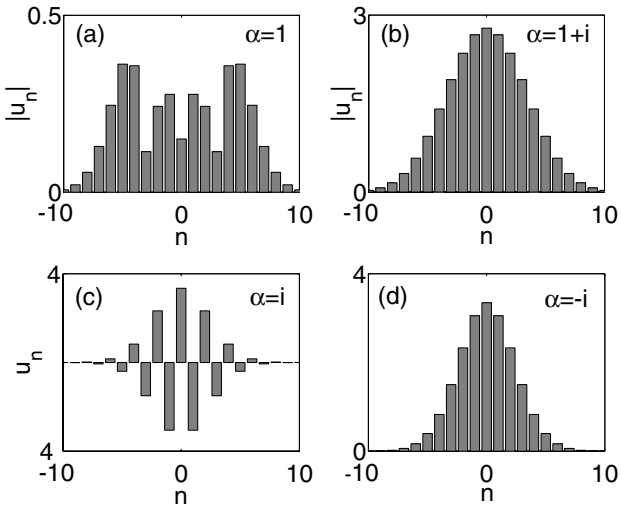

Fig. 2. Field profile of linear impulse response of the lattice at $z = 3$. In (**a**), $\epsilon = 0$, while in (**b**)–(**d**), $\epsilon = -1$

$$\mathrm{i}\dot{u}_n - \mathrm{i}\epsilon u_n + \alpha(u_{n+1} + u_{n-1}) + \beta n u_n = 0 \,, \tag{11}$$

where β is proportional to the modulation of the lattice. Since α_r represents the nearest-neighbor element coupling coefficient among the fundamental (zero-node) local modes, it is natural to assume that $\alpha_r > 0$.

We consider the possibility of Bloch oscillations in such a dissipative lattice. Extending the analysis of [27] to the complex domain, we find an exact solution for the impulse response of (11):

$$u_n(z) = J_n\left[\frac{4\alpha}{\beta}\sin\left(\frac{\beta z}{2}\right)\right]\exp\left[\frac{\mathrm{i}n}{2}(\beta z + \pi)\right]\mathrm{e}^{\epsilon z} \,. \tag{12}$$

Here, $J_n(x)$ is a Bessel function with a complex argument. Apart from the last exponential term in (12), the intensity of this wavefunction repeats itself after

$$Z_0 = 2\pi/\beta \,. \tag{13}$$

Apparently, the evolution of more complicated wavepackets will be given from superpositions of (12). The last term in (12) indicates that, on average, the power

$$P = \sum_n |u_n|^2 \tag{14}$$

will increase or decrease according to

$$\langle P \rangle \sim \exp(2\epsilon z) \,. \tag{15}$$

Notice that the average in (15) is taken over one period of the oscillations, Z_0:

$$\langle P \rangle = \frac{1}{Z_0} \int_z^{z+Z_0} P(z) dz \; . \tag{16}$$

In order to better understand the effect of the linear tilt displayed in (11), we will compare these results with the zero-tilt case. If $\beta = 0$, (11) has a complex dispersion curve allowing plane-wave solutions, as shown in the previous section. Obviously, under such conditions, where some modes are amplified more than others, periodic revivals of an input intensity pattern cannot occur.

If β is non-zero, the behavior of the system is very different. In Fig. 3, we can see the intensity evolution of a single waveguide excitation. The conservative case depicted on the left-hand-side is identical to the one discussed in [27]. Since there are no dissipation processes occurring in this case, the power is conserved with z. For the right-hand-side diagram, the coefficients are complex, i.e., $\alpha = 1 \pm \mathrm{i}0.4$ and $\epsilon = 0$, and so the total power is not locally conserved. The total power of the beam initially increases and attains a maximum at $z = Z_0/2$, but after that it decreases and the initial waveform recurs at $z = Z_0$. If ϵ is non-zero, the input beam will still demonstrate a similar behavior, apart from an average growth in its power, given by (15).

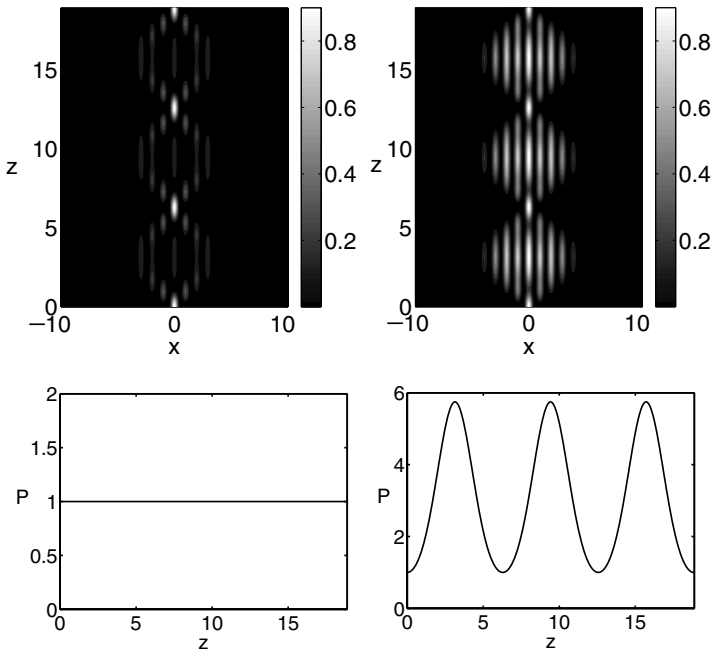

Fig. 3. Evolution of a single waveguide excitation when $\epsilon = 0$, $\beta = 1$. For the left-hand-side diagram, $\alpha = 1$, while for the right-hand-side one, $\alpha = 1 \pm \mathrm{i}0.4$

Qualitatively, this behavior can be understood on the basis that β causes the Bloch momentum θ to periodically scan the complex dispersion curves. As θ periodically oscillates in the Brillouin zone, the input beam experiences both normal and anomalous dispersion. In a similar way, due to the change in the value of θ, the growth rate is also periodically modulated. Interestingly enough, and since the impulse response excites the whole spectrum equally, the intensity profile is identical for both signs of α_i.

Another example is depicted in Fig. 4, where an initially-in-phase Gaussian beam of the form

$$u_n = \exp(-((n - n_0)/A)^2) \tag{17}$$

is launched into the lattice with $A = 2$. In this example, $\epsilon = 0$. On the left-hand-side, $\alpha = 1$ and so the power, P, remains invariant along z. In the middle plots, $\alpha = 1 + \mathrm{i}0.3$. Again, the $P - z$ diagram can be qualitatively explained. Since the initial configuration is in-phase, and $\alpha_i > 0$, the beam will initially experience loss. After some propagation length, the out-of-phase pattern grows and the power starts to increase with z. After approximately half a period, the phase of the pattern will shift and will have a tendency to become in-phase, thus experiencing losses. After one period, the input wavepacket is restored. The situation is different in the right-hand-side diagram, where $\alpha = 1 - \mathrm{i}0.3$. Since $\alpha_i < 0$, the in-phase patterns will have a tendency to gain power. Thus, as we can see from the $P - z$ diagram, the power increases with z when the beam is launched.

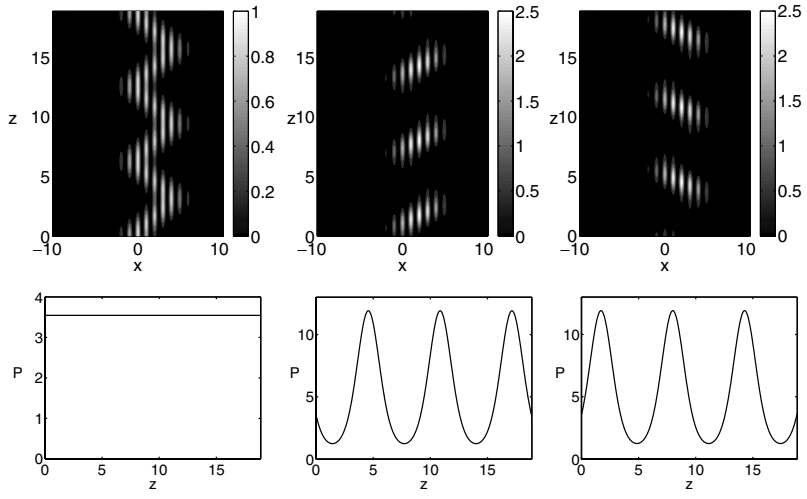

Fig. 4. Evolution of a Gaussian beam in a lattice with $\beta = 1$, $\epsilon = 0$ and $A = 2$, when (**a**) $\alpha = 1$ (*left-hand-side*), (**b**) $\alpha = 1 + \mathrm{i}3$ (*middle column*), and (**c**) $\alpha = 1 - \mathrm{i}3$ (*right-hand-side*)

This refractive index ladder also affects the stability of the zero background. Such an investigation is of interest when studying the stability of self-confined dissipative solitons. If $\beta = 0$, then the zero background should be stable for all values of θ, and so the necessary and sufficient stability condition is $\epsilon < -2|\alpha_i|$ [(5)]. However, if β differs from zero, then, due to the periodic variations of θ inside the Brillouin zone, stability can be established when the average growth is negative,

$$g_{\text{avg}} = \int_0^{\pi} g(\theta) d\theta = 2\pi\epsilon < 0 \ , \tag{18}$$

or

$$\epsilon < 0 \ . \tag{19}$$

By comparing the stability conditions, (5) and (19), it becomes apparent that a refractive index ladder improves the stability of the background.

4 Nonlinear Properties

4.1 Long Wavelength Regime

When a nonlinear wave is broad enough, i.e., it has an envelope that varies slowly with the index n, the long wavelength approximation can be applied. By studying the resulting continuous equation, many of the properties of the original discrete model, and especially those related to the Hopf bifurcation of the DS with the "zero amplitude" solution, can be revealed. Initially, we apply a phase transformation to the field,

$$u_n = v_n \exp(\mathrm{i}\theta n) \ , \tag{20}$$

resulting in

$$\mathrm{i}\dot{v}_n - \mathrm{i}\epsilon v_n + \alpha(u_{n+1}\mathrm{e}^{\mathrm{i}\theta} + u_{n-1}\mathrm{e}^{-\mathrm{i}\theta}) + p|u_n|^2 u_n + q|u_n|^4 u_n = 0 \ , \tag{21}$$

where θ is the linear phase difference between adjacent elements of the lattice. We can associate the discrete field, v_n, with a continuous function $v(x)$:

$$x_n = n\Delta x \ , \quad v(x_n) = v_n \ . \tag{22}$$

Without loss of generality, we will assume that $\Delta x = 1$. Of course, the solution of the original problem (21) can be reconstructed by sampling the continuous field $v(x)$ at the discrete points x_n. The field at lattice elements adjacent to n can be found be using the following Taylor expansion:

$$v_{n\pm1} = \sum_{n=0}^{\infty} \frac{(\pm 1)^n}{n!} \frac{\partial^n v(x)}{\partial x^n} \ . \tag{23}$$

Substituting (23) into (21), we find

$$\mathrm{i}\frac{\partial v}{\partial z} - \mathrm{i}\epsilon v + 2\alpha \sum_{n=0}^{\infty} \left[\frac{\cos\theta}{(2n)!} \frac{\partial^{2n} v}{\partial x^{2n}} + \frac{\mathrm{i}\sin\theta}{(2n+1)!} \frac{\partial^{2n+1} v}{\partial x^{2n+1}} \right] + p|v|^2 v + q|v|^4 v = 0 \; . \tag{24}$$

Equation (24) is equivalent to the following integro-differential equation:

$$\mathrm{i}\frac{\partial v}{\partial z} - \mathrm{i}\epsilon v + \frac{\alpha}{\pi} \int_{-\infty}^{\infty} dx' \int_{-\infty}^{\infty} dq \cos(\theta - q) e^{iq(x'-x)} v(x') + p|v|^2 v + q|v|^4 v = 0 \; . \tag{25}$$

We would like to mention that (25) is quite involved, and very little information about the dynamics of the DGL system can easily be derived from it. For this reason, we will further simplify (24) by employing the long-wavelength approximation.

In this latter regime, we assume that the discrete field varies quite slowly with the lattice index, i.e.,

$$|v_{n\pm1} - v_n| \ll 1 \; . \tag{26}$$

Utilizing (23) allows us to write the corresponding condition for the envelope:

$$\left| \sum_{n=1}^{\infty} \frac{(\pm 1)^n}{n!} \frac{\partial^n v(x)}{\partial x^n} \right| \ll 1 \; . \tag{27}$$

Assuming that v varies slowly with x as $v = v(\sigma x)$, where $\sigma \ll 1$, keeping terms up to the second order in σ, and applying the transformation $v(x,z) = U(x,z)\exp(i\alpha_r x)$, we arrive at:

$$\mathrm{i}\left(\frac{\partial U}{\partial z} + c\frac{\partial U}{\partial x} \right) - \mathrm{i}\epsilon' U + \alpha' \frac{\partial^2 U}{\partial x^2} + p|U|^2 U + q|U|^4 U = 0 \; , \tag{28}$$

where

$$\epsilon' = \epsilon - 2\alpha_i \cos\theta \; , \tag{29}$$

$$c = 2\alpha \sin\theta \; , \tag{30}$$

end

$$\alpha' = \alpha \cos\theta \; . \tag{31}$$

Changing the co-ordinate system to

$$X = x - cz, \quad Z = z \; , \tag{32}$$

we obtain the following cubic-quintic Ginzburg-Landau equation:

$$\mathrm{i}\frac{\partial U}{\partial Z} - \mathrm{i}\epsilon' U + \alpha' \frac{\partial^2 U}{\partial X^2} + p|U|^2 U + q|U|^4 U = 0 \; . \tag{33}$$

Equation (33) can help us understand the Hopf bifurcations of the soliton solutions with zero background. Exact soliton solutions of (33) were first found in [10]. Since we are interested in low-intensity solutions, it is natural to assume that the quintic term is negligible. Under this assumption, the bright soliton solution of (33) reduces to [7]

$$U(X,Z) = A\left[\mathrm{sech}(\eta X)\right]^{1+\mathrm{i}\mu}\,\mathrm{e}^{\mathrm{i}kZ}\ , \tag{34}$$

where

$$\mu = \frac{3b \pm \sqrt{9b^2+8a^2}}{2a}\ , \tag{35}$$

$$\eta^2 = \frac{\epsilon}{2\mu\alpha_r + \alpha_i(1-\mu^2)}\ , \tag{36}$$

$$k = \eta^2[\alpha_r(1-\mu^2)2\mu\alpha_i]\ , \tag{37}$$

$$A^2 = -\frac{3\mu\left(\alpha_r^2+\alpha_i^2\right)}{a}\eta^2\ , \tag{38}$$

$$a = p_r\alpha_i - p_i\alpha_r\ , \quad b = p_r\alpha_r - p_i\alpha_i\ . \tag{39}$$

Note that the plus/minus signs in (35) correspond to opposite signs of μ, of which only one satisfies the constraints $\eta^2 > 0$ and $A^2 > 0$. Using (38), we can see that the pulse width, $1/\eta$, of a soliton is inversely proportional to its amplitude A, and this, in turn, confirms our original assumption. Again, we would like to mention that the expressions derived here are valid for solutions that are sufficiently broad.

4.2 Highly-Confined Discrete Solitons

At the other extreme, i.e., when the discrete solitons are highly confined inside the lattice, these solutions are accurately described by

$$u = u_0\exp(-s|n| + \mathrm{i}\lambda z)\ , \tag{40}$$

where the parameters of the solution satisfy

$$\lambda + \mathrm{i}\epsilon = 2\alpha\cosh s \tag{41}$$

and

$$\sinh s = u_0^2\left(p + qu_0^2\right)/(2\alpha)\ . \tag{42}$$

In addition, one can obtain valuable information from the DS tails, since locally, $u_n \propto \exp(i\lambda z - s|n|)$ is satified. In this case, the relations/constraints of (8)–(9) hold true.

Using a perturbation method for the cubic model, one can accurately estimate:

$$u_0^2 = \left(\sqrt{\frac{\epsilon}{p_i}} - \sqrt{\frac{p_i}{\epsilon}} \frac{2p_r\alpha_r\alpha_i + p_i(\alpha_i^2 - \alpha_r^2)}{\epsilon(p_r^2 + p_i^2)} \right)^2 , \tag{43}$$

$$k = \frac{p_r\epsilon}{p_i} - 4\frac{\alpha_r\alpha_i(p_r^2 - p_i^2) + p_rp_i(\alpha_i^2 - \alpha_r^2)}{\epsilon(p_r^2 + p_i^2)} \tag{44}$$

$$u_{\pm 1} = \frac{\alpha}{p}\sqrt{\frac{p_i}{\epsilon}} \tag{45}$$

while similar expressions can be obtained for the quintic model. Again, for asymptotically-large values of the maximum intensity, $|u_0|^2$ is linearly-related to ϵ.

4.3 Discrete Solitons and Their Bifurcations

We will now investigate the structure, as well as some of the basic properties, of DS states existing in the GL lattice. To do so, we look for stationary localized modes, $u_n = \exp(i\lambda z)v_n$, of (1). Then the resulting algebraic system is solved numerically using the Newton iteration method. Note that (1) is subject to certain symmetries that can be used to reduce the parameter space of the system under study. We note that, by employing the phase transformation $u_n \to u_n \exp(i\pi n)$, along with $\alpha \to -\alpha$, (1) remains invariant. This, in turn, allows the one-to-one mapping $\alpha \leftrightarrow -\alpha$. Here, without any loss of generality, we assume that $\alpha_r > 0$. A second symmetry also exists, *viz.* $z \to -z$, and $u_n \to \exp(i\pi n)u_n$, $p \to -p$, $q \to -q$, which is used by applying an additional constraint, $p_r > 0$, to the system. In doing so, we consider immobile GL discrete solitons that reside either at the base ($\theta = 0$), or at the edge ($\theta = \pi$), of the Brillouin zone [37]. For $\theta = 0$, the DS bifurcates from the zero solution at $\epsilon = 2\alpha_i$, while in the case $\theta = \pi$, the DS bifurcates at $\epsilon = -2\alpha_i$. It is important to note that the existence of these two bifurcation points is a result of the periodicity introduced by the lattice model, and is in clear contrast to the continuous GL equation, where only one bifurcation occurs when the linear gain is zero.

In Fig. 5, typical co-dimension 1 bifurcation diagrams of the cubic DGL model are depicted. Figures 5a and c show bifurcations for DS located at the base of the Brillouin zone, whereas the curves of Fig. 5b and d correspond to the edge of the zone. As in the continuous GL case, these bifurcations are super-critical when $p_i > 0$ and sub-critical when $p_i < 0$. In all the bifurcation figures, solid and dash-dotted curves represent stable and unstable branches, respectively.

Close to the bifurcation point, the DS are quite broad, and, as a result, the numerically-found curves shown in Fig. 5 (with either $\theta = 0$ or $\theta = \pi$) are well-approximated by (33). Also, when the maximum intensity becomes relatively

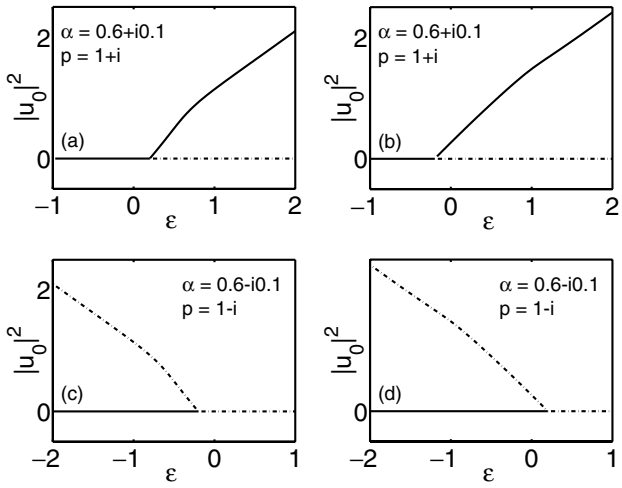

Fig. 5. Typical co-dimension 1 bifurcation diagrams of the cubic DGL model. In all the bifurcation figures, *solid* and *dash-dotted* curves represent stable and unstable branches, respectively

high, the solutions residing in the normal diffraction regime become highly localized inside the lattice. Figure 7a depicts such a highly-confined DS (at the base of the Brillouin zone), which is in excellent agreement with the analytical results of (40). On the other hand, in the anomalous discrete diffraction regime (at the edge of the Brillouin zone), a rather peculiar feature arises, *viz.* that the amplitude profile becomes broader and flatter with stronger chirp. We attribute this property to the rather involved energy flow within the GL DS under anomalous diffraction conditions. As an example, Fig. 7b shows the field of a high intensity DS in the anomalous diffraction regime that extends over seven lattice points. Similar types of solutions (flat-top) can also be found in the continuous Ginzburg-Landau model [11, 12]. On the other hand, these discrete flat-top solutions exist when the maximum intensity of the solutions is above a certain threshold, and their stability properties may be relevant to the modulational instability of the corresponding continuous-wave solutions. However, the possible bifurcation of these solutions is an issue that merits further investigation.

In general, the stability properties of the cubic DGL solitons can be identified from the corresponding bifurcation diagrams. A sub-critical DS will be unstable, whereas an unstable background can destabilize a super-critical DS. The properties of the bifurcation diagrams can be modified when the quintic term in (1) is non-zero. In fact, a saddle-node bifurcation emerges if the condition $p_i q_i < 0$ is satisfied. It is then of interest to determine the parameter space where absolutely stable DS exist. To realize this, it is necessary that the zero background, on which these discrete modes reside, is stable

for any perturbation frequency, i.e., $\epsilon < -2|\alpha_i|$. By taking this into account, and knowing, from standard bifurcation theorems, that stable and unstable manifolds alternate, one can then conclude that necessary conditions for DS stability are $p_i < 0$ and $q_i > 0$. In Fig. 6, such bifurcation diagrams of the quintic model, satisfying the necessary stability conditions, are presented. The curves shown in Fig. 6a and b correspond to the base and the edge of the Brillouin zone, respectively. The stability of these solutions has been investigated by performing numerical simulations. The DS shown in Fig. 7a lies on the upper branch of the bifurcation diagram and its stability has also been verified numerically. On the other hand, the solution shown in Fig. 7b happens to be unstable.

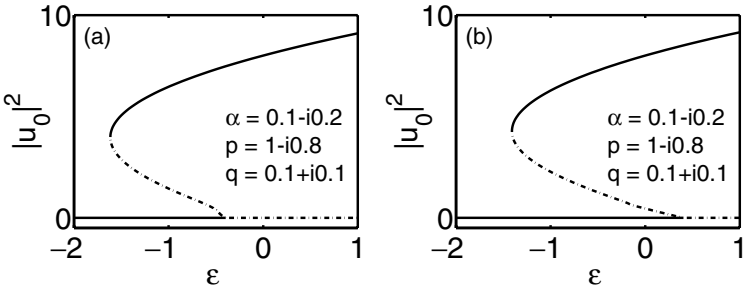

Fig. 6. Bifurcation diagrams of the quintic DGL equation (**a**) at the base and (**b**) at the edge of the Brillouin zone

We would also like to mention that, for a certain range of parameters, the DS solutions of the DGL equation can exhibit interesting behavior – the tails of the DS become very broad (occupying many lattice sites), whereas the central part of it is confined and displays a cusp-like feature, as shown in Fig. 8. Note that no such cusp soliton structures are possible in either the continuous GL regime or in DNLS lattices. To understand this behavior, one may use the relation $\lambda + \mathrm{i}\epsilon = 2\alpha \cosh s$, whence the rate of decay, s_r, of the soliton tails in (40) can be determined. In the case of Fig. 8, $s_r = 0.2$, which indeed justifies the slow field decay in the tails.

More complicated bifurcation diagrams that have no analogs in the continuous GL case also appear in the discrete model. For example, in Fig. 9 (normal diffraction regime), we can observe a sub-critical bifurcation that is followed by three successive saddle-node bifurcations. As a result, four different branches of non-zero solutions exist, allowing up to two stable DS for the same value of ϵ.

Except for the DS that are centered on a single lattice point (on-site), two different types of DS that are centered between two lattice points (intra-site) exist. These are characterized by the phase difference between the two central lattice points, and this can be either 0 or π when the solutions are

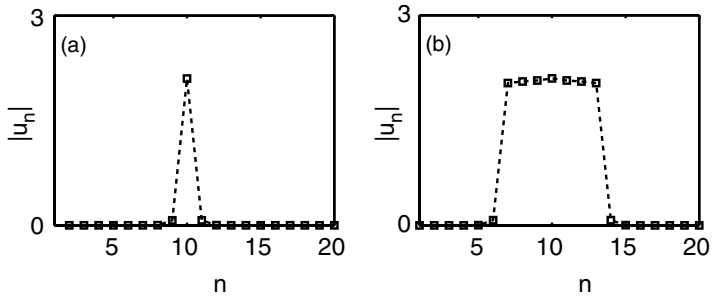

Fig. 7. (**a**) A highly-confined DS solution in the normal diffraction regime, and (**b**) the corresponding DS that resides at the edge of the Brillouin zone, when $\alpha = 0.1 - 0.2\mathrm{i}$, $p = 1 - \mathrm{i}0.8$, $q = 0.1 + 0.1\mathrm{i}$, $u_0 = 2.1$

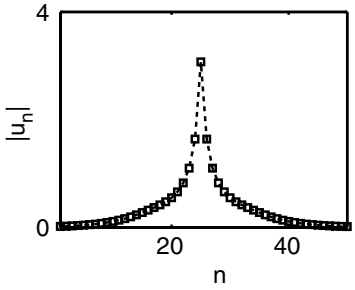

Fig. 8. A cusp-like DS solution for $\alpha = 0.4 - 2\mathrm{i}$, $p = 0.1 - 0.4\mathrm{i}$, $q = 0.43\mathrm{i}$ and $\epsilon = -0.4$

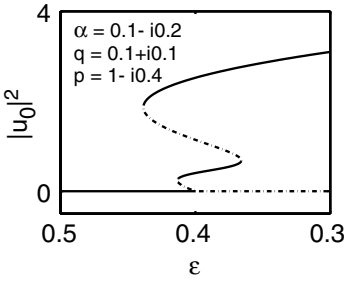

Fig. 9. A sub-critical bifurcation, followed by three successive saddle-node bifurcations at $\theta = 0$

highly confined. In the DNLS regime, the π-out-of-phase intra-site DS are known to be stable [38, 39] for relatively strong nonlinearities, whereas, the in-phase intra-site DS are always unstable because of oscillatory instabilities. However, in the DGL lattice system, we have identified regimes where both types of DS solutions are stable. In Fig. 10, such a stable intra-site in-phase

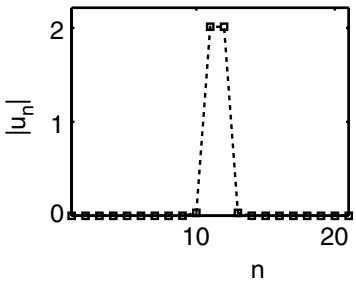

Fig. 10. In-phase stable intra-site DS for $\alpha = 0.1 - \mathrm{i}0.1$, $p = 0.2 - \mathrm{i}6$, $q = 0.2 + \mathrm{i}$, and $\epsilon = -8$

state is depicted. For these values of the parameters, both the in-phase and the out-of-phase DS are stable. Their intensity profiles are almost identical, and the main difference between them is the relative phase between the high-intensity lattice sites, which is 0 or π. The stability of these DS has been checked dynamically against symmetry-breaking perturbations. A more detailed stability analysis of these DS will be presented elsewhere.

Acknowledgements

This work was supported by an ARO MURI and by the Pittsburgh supercomputer center.

References

1. M. C. Cross and P. C. Hohenberg, Rev. Mod. Phys. **65**, 851 (1993).
2. Y. Kuramoto, *Chemical Oscillations, Waves and Turbulence*, (Springer, Berlin, 1984).
3. I. S. Aranson and L. Kramer, Rev. Mod. Phys. **74**, 99 (2002).
4. N. Akhmediev and A. Ankiewicz, *Solitons, Nonlinear pulses and beams*, (Chapman and Hall, London, 1997).
5. P. Manneville, *Dissipative Structures and Weak Turbulence*, (Academic, San Diego, 1990).
6. G. Nicolis *Introduction to Nonlinear Science*, (Cambridge University Press, Cambridge, 1995).
7. L. M. Hocking and K. Stewartson, Proc. R. Soc. London, Ser. A **326**, 289 (1972); N. R. Pereira and L. Stenflo, Phys. Fluids **20**, 1733 (1977).
8. K. Nozaki and N. Bekki, J. Phys. Soc. Jpn. **53**, 1581 (1984).
9. W. van Saarloos and P. C. Hohenberg, Physica D **56**, 303 (1992).
10. R. Conte and M. Musette, Physica D **69**, 1 (1993); P. Marcq, H. Chaté, and R. Conte, Physica D **73**, 305 (1994).
11. N. N. Akhmediev, V. V. Afanasjev and J. M. Soto Crespo, Phys. Rev. E **53**, 1190 (1996).

12. L. C. Crasovan, B. A. Malomed and D. Mihalache, Phys. Lett. A **289**, 59 (2001).
13. J. M. Soto-Crespo, N. Akhmediev and A. Ankiewicz, Phys. Rev. Lett. **85**, 2937 (2000).
14. P. S. Hagan, SIAM J. Appl. Math. **42**, 762 (1982).
15. L. C. Crasovan, B. A. Malomed and D. Mihalache, Phys. Rev. E **63**, 016605 (2001).
16. D. N. Christodoulides and R. I. Joseph, Opt. Lett. **13**, 794 (1988).
17. D. N. Christodoulides, F. Lederer and Y. Silberberg, Nature **424**, 817 (2003).
18. H. S. Eisenberg, Y. Silberberg, R. Morandotti, A. R. Boyd and J. S. Aitchison, Phys. Rev. Lett. **81**, 3383 (1998).
19. H. Willaime, O. Cardoso and P. Tabeling, Phys. Rev. Lett. **67**, 3247 (1991).
20. S. S. Wang and H. G. Winful, Appl. Phys. Lett. **52**, 1774 (1988); H. G. Winful and S. S. Wang, Appl. Phys. Lett. **53**, 1894 (1988).
21. K. Otsuka, *Nonlinear dynamics in optical complex systems*, (KTK Scientific Publishers, Tokyo, 1999).
22. K. Otsuka, Phys. Rev. Lett. **65**, 329 (1990); H. G. Winful and L. Rahman, Phys. Rev. Lett. **65**, 1575 (1990).
23. N. K. Efremidis and D. N. Christodoulides, Phys. Rev. E **67**, 026606 (2003).
24. K. Maruno, A. Ankiewicz and N. Akhmediev, Opt. Comm. **221**, 199 (2003).
25. K. Staliunas, Phys. Rev. Lett. **91**, 053901 (2003).
26. N. K. Efremidis and D. N. Christodoulides, *Bloch oscillations in dissipative lattices*, in preparation.
27. U. Peschel, T. Pertsch and F. Lederer, Opt. Lett., **23**, 1701 (1998).
28. T. Pertsch, P. Dannberg, W. Elflein, A. Brüer and F. Lederer, Phys. Rev. Lett. **83**, 4752 (1999).
29. R. Morandotti, U. Peschel, J. S. Aitchison, H. S. Eisenberg and Y. Silberberg, Phys. Rev. Lett. **83**, 4756 (1999).
30. C. Kittel, *Introduction to Solid State Physics* (Wiley, New York, 1986).
31. E. A. Ultanir, D. Michaelis, F. Lederer and G. I. Stegeman, Opt. Lett. **28**, 251 (2003).
32. B. P. Anderson and M. A. Kasevich, Science **282**, 1686 (1998).
33. A. Trombettoni and A. Smerzi, Phys. Rev. Lett. **86**, 2353 (2001).
34. B. Kneer, T. Wong, K. Vogel, W. P. Schleich and D. F. Walls, Phys. Rev. A **58**, 4841 (1998).
35. F. T. Arecchi, J. Bragard and L. M. Castellano, In: *Bose-Einstein Condensates and Atom Lasers*, edited by S. Martellucci, A. N. Chester, A. Aspect, and M. Inguscio. (Kluver, New York, 2002).
36. F. Bloch, Z. Phys., **52**, 555 (1928).
37. Y. S. Kivshar, Opt. Lett. **18**, 1147 (1993).
38. S. Darmanyan, A. Kobyakov and F. Lederer, Zh. ksp. Teor. Fiz. **113**, 1253 (1998) [Sov. Phys. JETP **86**, 682 (1998)].
39. P. G. Kevrekidis, A. R. Bishop and K. O. Rasmussen, Phys. Rev. E **63**, 036603 (2001).
40. N. K. Efremidis and D. N. Christodoulides, Phys. Rev. E **65**, 056607 (2002).